Journal of Soils and Sediments (2020) 20:3217–3229
https://doi.org/10.1007/s11368-020-02650-y

SOILS, SEC 5 • SOIL AND LANDSCAPE ECOLOGY • RESEARCH ARTICLE

The influence on biosorption potentials of metal-resistant bacteria *Enterobacter* sp. EG16 and *Bacillus subtilis* DBM by typical red soil minerals

Wenling Feng[1] · Yaying Li[1,2] · Zhiyun Lin[1] · Yang Luo[1] · Shizhong Wang[1,2] · Rongliang Qiu[1,2]

Received: 19 December 2019 / Accepted: 27 April 2020 / Published online: 12 May 2020

Abstract

Purpose Due to the inevitable interaction between bacteria and soil minerals, whether bacteria could exert the excepted functions in the soil is yet to be confirmed and how minerals affect biosorption potential is needed to be investigated. The purposes of this study were to explore the adsorption behavior and mechanism of metal-resistant bacteria attaching to typical red soil minerals under different conditions and to discuss whether biosorption potential would be altered after the addition of functional bacteria to soil.

Materials and methods Here, we tested equilibrium adsorption along with zeta potential analysis, scanning electron microscopy (SEM), Fourier transform infrared spectra (FTIR), and desorption to investigate the adsorption of two metal-resistant bacteria (Gram-negative *Enterobacter* sp. EG16 and Gram-positive *Bacillus subtilis* DBM) onto typical red soil minerals including goethite, kaolinite, and gibbsite under different environmental factors.

Results and discussion We found that the minerals adsorbed more EG16 cells than DBM, and the adsorption capacities followed the sequence of goethite > kaolinite > gibbsite. Both the surfaces of bacteria and mineral were pH-dependent in our tested pH range (4.0–7.0), and the maximum adsorption was at pH 4.0. Increasing ionic strength resulted in less adsorption of bacteria onto goethite, whereas bacterial adsorption onto kaolinite was the opposite. These observations elucidated that electrostatic interaction was the dominant contributor. The adsorption conformed to the Langmuir and pseudo-second-order kinetic model implying chemical adsorption, and the result of FTIR also supported that. Desorption experiment has suggested the significant contribution of electrostatic force and the minor dominator of functional groups for bacteria–mineral combination.

Conclusions The results of this study indicated that electrostatic interaction was the dominant contributor to bacteria–mineral combination and functional groups coordination contributed less than 10%. This finding suggested most adhered bacteria could still provide active sites for heavy metal biosorption. Thus, although 50–90% of added functional bacteria has adhered to minerals, the bacteria–mineral combination had a limited impact on biosorption.

Keywords Metal-resistant bacteria · Red soil minerals · Adsorption potentials · Microbial-assisted phytostabilization

Responsible editor: Yuan Ge

Electronic supplementary material The online version of this article (https://doi.org/10.1007/s11368-020-02650-y) contains supplementary material, which is available to authorized users.

✉ Yaying Li
liyaying3@mail.sysu.edu.cn

[1] School of Environmental Science and Engineering, Sun Yat-sen University, Guangzhou 510275, China

[2] Guangdong Provincial Key Laboratory of Environmental Pollution Control and Remediation Technology, Guangzhou 510275, China

1 Introduction

Red soil is distributed widely in tropical and subtropical regions, such as south China (Liu et al. 2010). These red soil regions contain abundant mineral resources, accompanied by extensive mining activities, which lead to severe heavy metal contamination, threatening human health (Lu et al. 2015). Phytostabilization is a commonly used bioremediation technology that immobilizes soil heavy metals with stress-resistant plants (Wang et al. 2017). However, under high heavy metal stress, plants usually have the shortcomings of slow growth and low biomass which limit the efficiency of bioremediation

(Turgay and Bilen 2012). To address this problem, eco-friendly and effectively, assisted phytoremediation with functional metal-resistant bacteria is one of the most promising approaches (Rajkumar et al. 2012). Some metal-resistant bacteria can change heavy metal bioavailability, mobility, and speciation by biosorption, bioaccumulation, and metal reduction, which could effectively reduce metal toxicity to both plants and bacteria (Chatterjee et al. 2009; Joshi and Juwarkar 2009; Juwarkar et al. 2007; Vivas et al. 2006). Besides, some metal-resistant bacteria can improve plant growth by producing plant growth regulators, such as indole-3-acetic acid (IAA) and 1-aminocyclopropane-1-carboxylate (ACC) deaminase (Luo et al. 2011; Ma et al. 2011; Wang et al. 2011).

To date, research on microbial-assisted phytoremediation for heavy metal contaminated soils has focused primarily on how plant and microorganisms interact (Belimov et al. 2005; Chen et al. 2016b), how microbes promote plant growth, and how bacteria help to immobilize heavy metal (Sinha and Mukherjee 2008). However, almost 80–90% of microorganisms added into soil ultimately adhered to soil minerals rather than be in soil solution. The adsorption of metal-resistant bacteria onto mineral surfaces is an initial step in bacterial colonization in soil (Ams et al. 2004). By this interaction, it may influence surface properties, such as chargeability and surface sites concentration of both materials, which might affect biosorption for heavy metals (Moon and Peacock 2013; Wang et al. 2016). Thus, it is desirable to understand the mechanism of adsorption of metal-resistant bacteria onto red soil minerals and to analyze the possible influenced portion within bacteria–mineral combination for biosorption potentials.

On the one hand, present research shows that adsorption of bacteria onto minerals can be affected by many environmental factors, such as pH, ionic strength, adsorption time, and bacteria–mineral ratios. Zhang et al. (2014) reported that *Escherichia coli* O157:H7 attachment onto kaolinite and goethite surfaces increased as pH decreased from 10.0 to 3.0. Jiang et al. (2007) also observed the same results for pH study from 10.0 to 2.0. Rong et al. (2010) and Cai et al. (2013) found opposite trends of Gram-negative bacteria adhered to goethite with same increasing ionic strength from 1 to 100 mM K^+. However, on why the adsorption trend went on opposite directions under one same factor, there was no consistent answer.

On the other hand, some studies suggested that adsorption of bacteria onto minerals also can be affected by the cell wall characteristics and structure of bacteria as well as by the types and surface properties of minerals. Ams et al. (2004) observed that compared to *Pseudomonas mendocina* (Gram-negative), more *Bacillus subtilis* (Gram-positive) had attached to Fe-coated quartz surfaces, owing to cell wall structure differences. Jiang et al. (2007) found that *Pseudomonas putida* preferred to attach on the surface of goethite, followed by surface of kaolinite and montmorillonite, due to different mineral types and surface properties. Until now, it is yet to confirm how cell wall differences and mineral types influence on bacteria–mineral interactions.

Most studies on the bacteria–mineral combination only focus on the influence on the adsorption behavior of different factors mentioned above. Few have elucidated the different combination ways of bacteria and minerals and the contribution of each way of combination, which may affect the surface properties and adsorption sites of metal-resistant bacteria. At present, the main unresolved questions are as follows: (1) how the essential factors, such as ionic strength and cell wall structures, influence bacterial adhesion to minerals; (2) how these factors impact on the combination modes and whether a consistent combining pattern between specific bio- and mineral surface; (3) whether the combination modes alter biosorption. A comprehensive analysis is needed.

The objective of this study was to investigate whether minerals would affect biosorption potential of metal-resistant bacteria. The effects of different adsorption conditions (pH, ionic strength, interaction time, and bacteria–mineral ratios) on the adsorption of two metal-resistant bacteria (Gram-negative *Enterobacter* sp. EG16 and Gram-positive *Bacillus subtilis* DBM) by three typical red soil minerals (kaolinite, goethite, and gibbsite) were measured. Two metal-resistant strains have been confirmed their effectivity on biosorption and plant growth promotion (Bai et al. 2014; Chen et al. 2016b). Due to desilicified allitization of red soils in south China, clay minerals (primarily kaolinite) and iron-alumina oxides (goethite and gibbsite) were chosen as tested typical red soil minerals (Cheng et al. 2017). Scanning electron microscopy, Fourier transform infrared spectroscopy, and zeta potential were used to provide insight into the mechanisms of adsorption of metal-resistant bacteria onto minerals, and desorption experiment was carried out to quantify the contribution of different adsorption approaches.

2 Materials and methods

2.1 Culture of bacteria and preparation of bacterial suspension

The bacterial strains used in this study were isolated and tested by our laboratory, Guangdong Provincial Key Lab of Environmental Pollution Control and Remediation Technology, Sun Yat-sen University, Guangzhou, China. The heavy metal-resistant strain *Enterobacter* sp. EG16 (a Gram-negative strain) was isolated from the rhizosphere of *Hibiscus cannabinus* growing in multi-metal polluted mine tailings, and *Bacillus subtilis* DBM (a Gram-positive strain) was isolated from multi-metal contaminated paddy soil. We

have proven that EG16 has the capacity of accumulating Cd by surface biosorption and intracellular accumulation, and promoting plant growth by secreting siderophores and botanical hormone IAA (Chen et al. 2016a; Chen et al. 2016b). DBM was confirmed its tolerance to Cd, Pb, Cu, and Zn and could synthesize IAA and ACC deaminase and promote plant growth (Bai et al. 2014).

Bacteria were inoculated in beef extract-peptone medium (beef extract 5.0 g, peptone 10.0 g, NaCl 5.0 g, water 1 L, pH 7.2) and shaken at 30 °C and 150 rpm for 24 h to stationary phase. The bacterial cells were collected by centrifugation at 4000 rpm for 10 min repeatedly. Then washed it three times with sterilized distilled-deionized (DDI) water to remove the remaining medium and resuspended in 0.2 mol L^{-1} phosphate buffer solution to obtain bacterial suspension with an OD_{600} value equal to 1.0. The specific surface area (SSA) of dead cell powder after freeze-drying (Table S1) was determined using N_2 adsorption (Guangzhou Analytical Instrument Company).

2.2 Mineral preparation

Tested minerals (goethite, kaolinite, and gibbsite) were purchased from Sigma-Aldrich and ground to pass a 100-mesh sieve (particle size < 150 μm) before used. The specific surface area of goethite, kaolinite, and gibbsite (Table S1) was determined using N_2 adsorption amount (Guangzhou Analytical Instrument Company). X-ray diffraction analysis (Fig. S1) confirmed that three tested minerals had high purity and were proper for the subsequent tests.

2.3 Bacteria–mineral adsorption experiments

Batch experiments were performed to measure the adsorption of bacteria onto minerals as a function of pH, ionic strength, adsorption time, and bacteria–mineral ratio at 150 rpm and 25 °C. Ten-milliliter aliquot of $OD_{600} = 1.0$ (0.50 mg mL^{-1}) bacterial suspension and 0.01-g mineral were mixed in a 50-mL centrifuge tube. The mixture was adjusted to desired initial pH values (4.0, 5.0, 5.5, 6.0, 7.0) using 0.1 M NaOH or HNO_3 at 0.01 M KNO_3 and analyzed adsorption percentage at equilibrium. We also tested adsorption equilibriums under different ionic strength of 1, 10, 50, and 100 mM KNO_3 at pH 5.5. In the bacteria–mineral ratio experiment, 0.01-g tested minerals were mixed with 0, 0.017, 0.033, 0.050, 0.067, 0.167, 0.267, 0.333, and 0.500 mg mL^{-1} bacteria suspension, equal to ratio of 0, 0.025:1, 0.05:1, 0.075:1, 0.1:1, 0.25:1, 0.4:1, 0.5:1, and 0.75:1, in a 50-ml centrifuge tube at 0.01 M KNO_3 and pH 5.0 to a total volume of 15 ml. For the kinetic experiment, adsorption percentage was analyzed for different reaction times of 0, 1, 3, 5, 10, 15, 30, 60, 90, and 120 min at 0.01 M KNO_3 and pH 5.0.

The separation of bacteria–mineral composites and unabsorbed fraction was accomplished using sucrose step-gradient centrifugation (Rong et al. 2008). When adsorption reached equilibrium, 4 ml 60% w/w sucrose solution was injected through the bottom of the tested tube and centrifuged at 4000 rpm for 20 min. Due to density differences, bacteria–mineral composites can be collected at the bottom of the tested tube, while unabsorbed bacteria were separated in the supernatant above the sucrose layer (Yee et al. 2000). Unattached bacteria were pipetted out and pyrolyzed by 0.5 M NaOH at 100 °C for 30 min (Jiang et al. 2007), of which the protein content was determined using Coomassie bright blue staining at 595-nm wavelength (Zhang et al. 2014). Preliminary experiment confirmed a good linear relationship between bacterial protein content and bacterial quantity with R^2 over 0.96 (Fig. S2). The adsorption percentage was calculated by subtracting the unabsorbed bacteria amount from the initial amount.

2.4 Bacteria–mineral desorption experiment

Desorption experiment of bacteria–mineral composites was carried out at pH 5, right after adsorption of bacteria, and minerals have reached equilibrium at pH 5, 0.01 M KNO_3 under 25 °C. Bacteria–mineral composites were collected by centrifugation at 4000 rpm for 10 min. Then, the composites were resuspended respectively in 15 mL milli-Q water or 0.1 mol L^{-1} EDTA-Na_2 and desorbed for 1 h with 150 rpm at pH 5, 0.01 M KNO_3. After desorption, unattached bacteria in the supernatant were pyrolyzed and quantified using Coomassie staining method. Subtracted the unattached bacteria amount from that of adsorbed bacteria, the number of bacteria desorbed by two eluants can be obtained, and the proportion of each combination ways can be calculated. The part desorbed by milli-Q water indicates that the composites formed by physical effects, while EDTA-Na_2 can desorb the part that combined by physical adsorption, and functional groups coordination (Bai et al. 2014; Fang et al. 2011). By subtracting the water-desorbed amount from EDTA-Na_2 desorbed amount, this part was obtained as chemical effects. The portion that cannot be desorbed by two eluants is considered to have spatial hindrance, such as insertion.

2.5 Experiments on micro-mechanism of bacteria–mineral adsorption

2.5.1 Zeta potential

Zeta potentials of bacteria, minerals, and bacteria–mineral composites were measured by zeta potential analyzer (Zetasizer Nano ZS90) at adsorption equilibrium under a range of pH (4.0, 5.0, 5.5, 6.0, 7.0), at 10 mM KNO_3 or a range of ionic strength (1, 10, 50, and 100 mM) at pH 5.5 at 25 °C.

2.5.2 Scanning electron microscopy

The morphology of minerals and bacterial–mineral composites (with saturated adsorption at pH 5.0, 10 mM KNO_3, 25 °C) was examined by scanning electron micrography (SEM, Quanta 400, FEI Co., Hillsboro, OR, USA). Sample preparation was done using modified fixation method (Hong et al. 2018), in which cells and complexes were fixed with 2.5% glutaraldehyde for 2 h at 4 °C, washed three times with phosphate buffer and then dehydrated in gradient ethanol (30%, 50%, 70%, 90%, and 100%) for 15 min at each step. Samples were treated 3 times with tert-butanol, 15 min each time, and the mixed suspension was dripped on a tin foil paper, freeze-dried and sputter-coated with gold under vacuum.

2.5.3 Fourier transform infrared spectrography

Bacteria, minerals, and bacteria–mineral composites (with saturated adsorption at pH 5.0, 10 mM KNO_3 and 25 °C) were freeze-dried for 24 h. The lyophilized samples were mixed with KBr powder (1:100, w/w), ground and compressed in a hydraulic press. The infrared spectra of bacteria, mineral, and the bacteria–mineral composites were recorded by a Fourier transform infrared (FTIR) spectrometer (EQUINOX 55, Bruker, Germany), operating in the range of 400–4000 cm^{-1} with a scan rate of 0.2 cm sec^{-1}.

2.6 Statistical analysis

All experiments were carried out in triplicate, and the reported results represent the mean of three values ± standard deviations. Analysis of variance and Duncan's multiple range test at $p < 0.05$ were used to compare treatment means. All statistical analyses were carried out using SPSS 20.0.

3 Results

3.1 Surface characteristics of bacteria and tested materials

In Fig. 5, we could observe the shapes of three tested minerals that goethite was fine acicular shape crystal, kaolinite was flake-shape, and gibbsite was columnar crystal with a smooth surface. Their specific surface areas (Table S1) were 10.45, 8.89, and 0.44 $m^2\ g^{-1}$, respectively. The XRD (Fig. S1) and FTIR (Table 2) results illustrated the chemical components and surface groups of their structures. The bands of goethite at 607 cm^{-1}, 798 cm^{-1}, and 904 cm^{-1} indicating a FeO_6 core with -O-/-OH encircled structure. The vibration recognized a double-layer structure of kaolinite as $AlO(OH)_x$ and SiO_4 with -OH on Al sides at 469 cm^{-1}, 537 cm^{-1}, 1006 cm^{-1}, and 912 cm^{-1}. The vibration at 450 cm^{-1} and 537 cm^{-1} implied columnar gibbsite of $AlO(OH)_x$ with -O-/-OH skeleton. As presented in Fig. 2, zeta potentials of both bacteria and kaolinite were negative. At the same time, those of goethite and gibbsite were positive, indicating electrostatic attraction between bacteria and goethite or gibbsite but electrostatic repulsion between bacteria and kaolinite. The smaller absolute value of goethite and bacteria implied their aggregation potentials. As infrared spectra (Fig. S4) presented, our tested bacterial surfaces both contained carboxyl, hydroxyl, carbonyl, amide, and phosphate groups provided by surface proteins, polysaccharides, phospholipid, and peptidoglycan, marked by the bands at 3300 cm^{-1} (Nath and Ray 2015), 2926 cm^{-1} (Das and Guha 2007), 1653 cm^{-1} and 1541 cm^{-1} (Doshi et al. 2007), 1453 cm^{-1} (Ueshima et al. 2008), 1394 cm^{-1} (Cao et al. 2011), and 1236 cm^{-1} and 1077 cm^{-1} (Cao et al. 2011; Loukidou et al. 2004).

3.2 Effect of pH on adsorption of bacteria by red soil minerals

The results showed that the adsorption capacity of three tested minerals for two bacterial strains decreased with increasing pH from 4.0 to 7.0 (Fig. 1a). Adsorption of EG16 onto goethite, kaolinite, and gibbsite decreased from 79, 56, and 39 to 59, 18, and 13%, respectively, while the corresponding decreases for DBM were from 73 to 54% on goethite, from 53 to 17% on kaolinite, and from 39 to 10% on gibbsite. The effect of pH on adsorption was similar between the Gram-positive strain DBM and Gram-negative strain EG16. For kaolinite and gibbsite, within the range of pH 4.0–6.0, the pH effect was most pronounced that adsorption for EG16 and DBM had been decreased 23–36% and 27–35% respectively. For goethite, the influence of pH on adsorption was strongest between pH 5.0 and 5.5. The significant decrease may be related to surface charge changes, which was consistent with the change of zeta potentials.

Significant decreasing zeta potentials were observed for all samples with increasing pH (Fig. 2), which may be related to the deprotonation of surface functional groups with additional bases (Zhao et al. 2012). Besides, zeta potentials of all composites changed to negative charges, indicating adsorbed bacteria had covered and masked most surface area of tested minerals. It is worth noting that goethite–bacteria composites changed from positive charge to negative charge from pH 4.0 to 5.0, accompanied by a steep decline to the value similar to those of bacteria. Comparing all formed composites, the absolute values of zeta potential followed the order of kaolinite-EG16 > kaolinite-DBM > goethite-EG16 > goethite-DBM > gibbsite-EG16 > gibbsite-DBM, which all within 20, implying possible aggregation and favorable for metal immobilization.

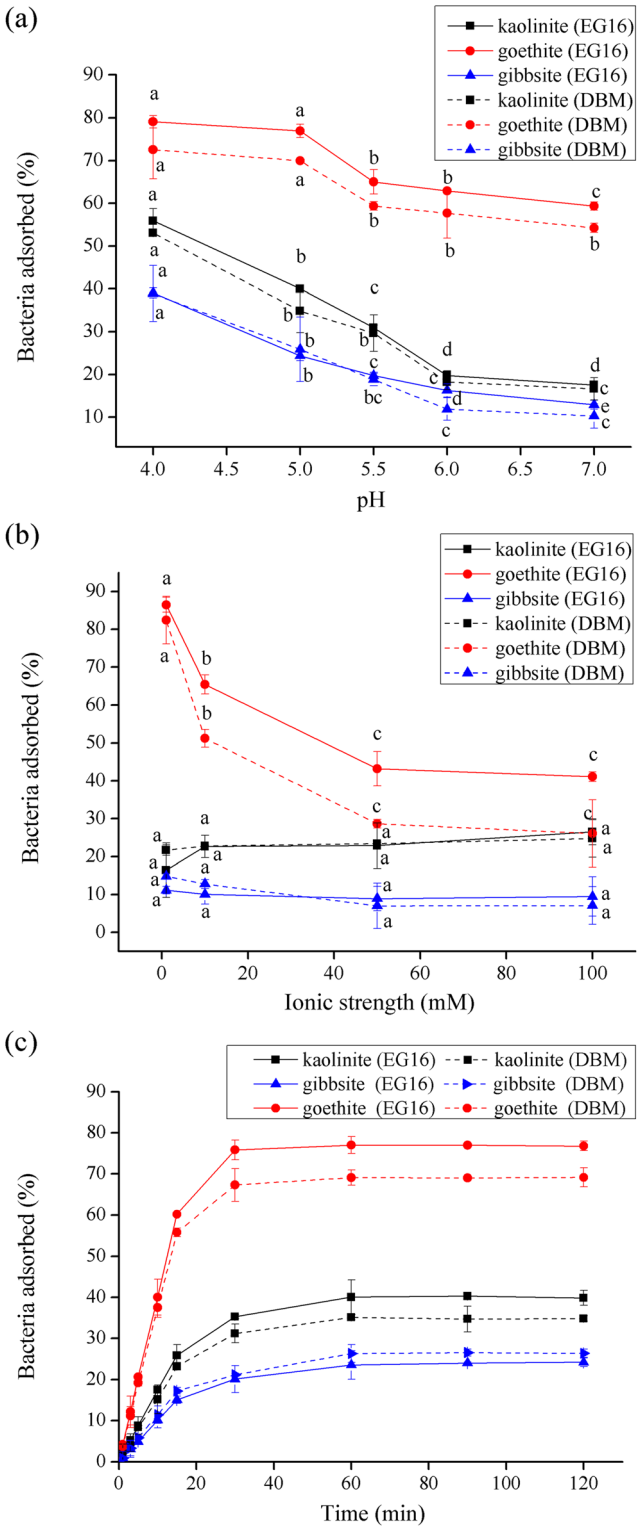

Fig. 1 Impact of different pH (**a**), ionic strength (**b**), and interaction time (**c**) on goethite, kaolinite, and gibbsite adsorption for bacteria *Enterobacter* sp. EG16 and *Bacillus subtilis* DBM

3.3 Effect of ionic strength on adsorption of bacteria by red soil minerals

The adsorption of goethite for both EG16 and DBM decreased significantly from 86.5 to 43.2% for EG16 and from 82.4 to 28.6% for DBM with increasing ionic strength from 1 to 50 mM KNO_3 (Fig. 1b). In contrast, the adsorption capacity of kaolinite and gibbsite for two bacterial strains has no evident changes within tested ionic strength range, except a minor increase for that of kaolinite at the very beginning. Their changing zeta potentials had supported these trends (Fig. 2). For natural negatively charged materials, significant increasing zeta potentials have been observed with increasing ionic strength, possibly covered by a large amount of K^+ while for minerals with positive charge surface, a significant decreasing trend was found.

3.4 Adsorption kinetics and isothermal adsorption

Adsorption trends of tested minerals for EG16 and DBM under different reaction time were the same (Fig. 1c). The adsorption proceeded rapidly in the initial 15 min that 60%, 25%, and 15% EG16 and 55%, 22%, and 18% DBM had been adsorbed on goethite, kaolinite, and gibbsite. Subsequently, adsorption began to slow down. Bacterial adsorption on goethite reached equilibrium in approximately 30 min while the corresponding adsorption saturation for kaolinite and gibbsite delayed till 60 min. The shorter saturated time of adsorption on goethite was probably due to its acicular structure and larger surface area and also the strong electrostatic attraction between positively charged goethite and negatively charged bacteria. From the linear fitting of kinetics (Table 1, Fig. S3), pseudo-second-order kinetic model better reflected the observed adsorption behavior ($R^2 > 0.97$) compared to pseudo-first-order kinetic model. Also, the q_e values calculated by pseudo-second-order kinetic approximated the experimental results.

As for the adsorption isotherms (Fig. 3), it showed that the quantity of adsorbed bacteria increased with larger bacteria–mineral ratios. The approximate adsorption equilibrium ratios of goethite, kaolinite, and gibbsite for EG16 were 0.75:1, 0.4:1, and 0.4:1, respectively. And for DBM, the approximate adsorption equilibrium ratios of goethite, kaolinite, and gibbsite were 0.5:1, 0.4:1, and 0.4:1, respectively. The maximum capacities of EG16 on goethite, kaolinite, and gibbsite were 128.17%, 117.23%, and 100.29% of DBM, respectively. Comparing the adsorption capacity of three tested minerals, there was a decreasing order of goethite > kaolinite > gibbsite. All these adsorptions can be well simulated by the Langmuir model with higher correlation coefficients (all > 0.94) than those of the Freundlich model (Table 1), indicating single-layer chemical adsorption. The maximum experimental capacities of goethite, kaolinite, and gibbsite reached 56.2%, 79.4%, and 79.9% of theoretical Q_{max} values for EG16, and 66.6%, 81.8%, and 82.3% of that for DBM.

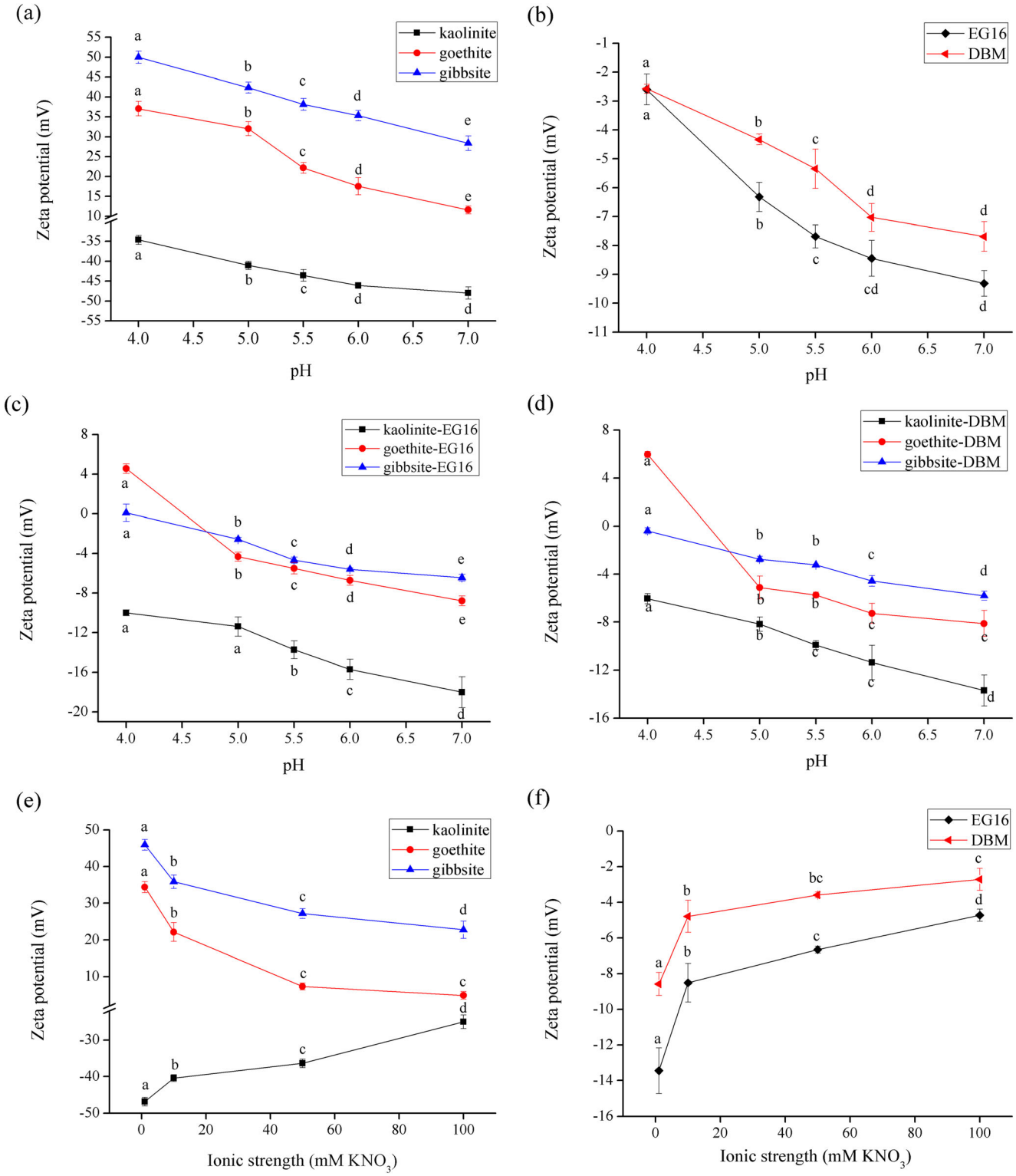

Fig. 2 Zeta potential of bacteria (EG16 and DBM), minerals (goethite, kaolinite, and gibbsite), and mineral–bacterial composites as a function of pH (**a**, **b**, **c**, **d**) and ionic strength (**e**, **f**)

3.5 Desorption of bacteria from tested minerals

The results of desorption showed (Fig. 4) that bacteria–mineral composites were mainly formed through electrostatic combination (or hydrogen bonding) and insertion, with a small portion of functional groups binding. For both goethite–bacteria composites and kaolinite–bacteria composites, insertion might be the major forming approach, occupied

Table 1 Equations and parameters of kinetics and isothermal adsorption fitting of bacteria and mineral combination

	Bacteria	Mineral	Experimental	Pseudo-first-order		Pseudo-second-order			
			q_e(mg g^{-1})	Equation	R^2	Equation	R^2	$q_{e,cal}$(mg g^{-1})	k_2
Kinetic model	EG16	Goethite	386.65	$dq_t/dt = k_1(q_e\text{-}q_t)$① $\ln(q_e\text{-}q_t) = \ln q_e\text{-}k_1t$②	0.811	$dq_t/dt = k_2(q_e\text{-}q_t)^2$① $t/q_t = 1/k_2q_e^2 + t/q_e$ ②	0.984	434.78	0.0002
		Kaolinite	201.40		0.945		0.981	243.90	0.0002
		Gibbsite	120.86		0.970		0.981	149.25	0.0003
	DBM	Goethite	346.26		0.825		0.984	400.00	0.0002
		Kaolinite	175.70		0.970		0.986	204.08	0.0003
		Gibbsite	132.75		0.966		0.974	163.93	0.0003
Isothermal model	Bacteria	Mineral	Experiment	Freundlich		Langmiur			
			Q_{max} (mg g^{-1})	Equation	R^2	Equation	R^2	Q_{max} (mg g^{-1})	K
	EG16	Goethite	300.51	$Q_e = KC_e^{1/n}$	0.942	$Q_e = Q_{max}KC_e/(1 + KC_e)$	0.984	534.53	3.10
		Kaolinite	202.42		0.851		0.948	255.04	9.40
		Gibbsite	128.42		0.892		0.978	160.74	11.86
	DBM	Goethite	277.90		0.905		0.974	417.05	5.47
		Kaolinite	177.94		0.859		0.954	217.56	10.48
		Gibbsite	131.88		0.862		0.971	160.27	13.24

Note: q_t represents the adsorbed amount when the adsorption time is t (mg g^{-1}); q_e is the adsorption capacity at equilibrium (mg g^{-1}); k_1 represents the rate constant of first order kinetics (1 min^{-1}); k_2 represents the rate constant of second order kinetics (g (mg min)$^{-1}$); ① is differential equations and ② is integral expression formulas. Time t is the x-coordinate value, $ln(q_e\text{-}q_t)$ is the y-coordinate value, and the parameters of the pseudo-first-order dynamic equation can be obtained by linear equation fitting. Similarly, time t as the x-coordinate value and t/q_t as the y-coordinate value, the parameters of the pseudo-second-order dynamic equation can be obtained by using linear equation fitting. $q_{e,exp}$, experimental maximum adsorption capacity; $q_{e,cal}$, theoretical maximum adsorption capacity from kinetic modeling; R^2, correlation coefficient. Q_e represents adsorbed bacteria onto minerals (mg g^{-1}); C_e is the equilibrium concentration of bacteria (mg mL^{-1}); Q_{max} denotes the maximum adsorption amount of bacteria on minerals (mg g^{-1}); K is the equilibrium constant (mL mg^{-1}); n is a constant

88.5% and 60.8% for EG16 and 83.1% and 54.7% for DBM respectively, followed by the electrostatic combination (or hydrogen bonding). For gibbsite–bacteria composites, an opposite result was observed that electrostatic combination was the dominant contributor, accounting for 62.20% EG16 and 63.49% DBM. Chemical adsorption via functional groups occupied a portion in DBM-mineral composites modes (Fig. 4), while that of EG16–mineral composites was rare or almost absent. This difference probably related to the stretched-out teichoic acid on the cell wall of Gram-positive strain DBM (Fig. 5) (Kulczycki et al. 2002), providing substantial active functional groups.

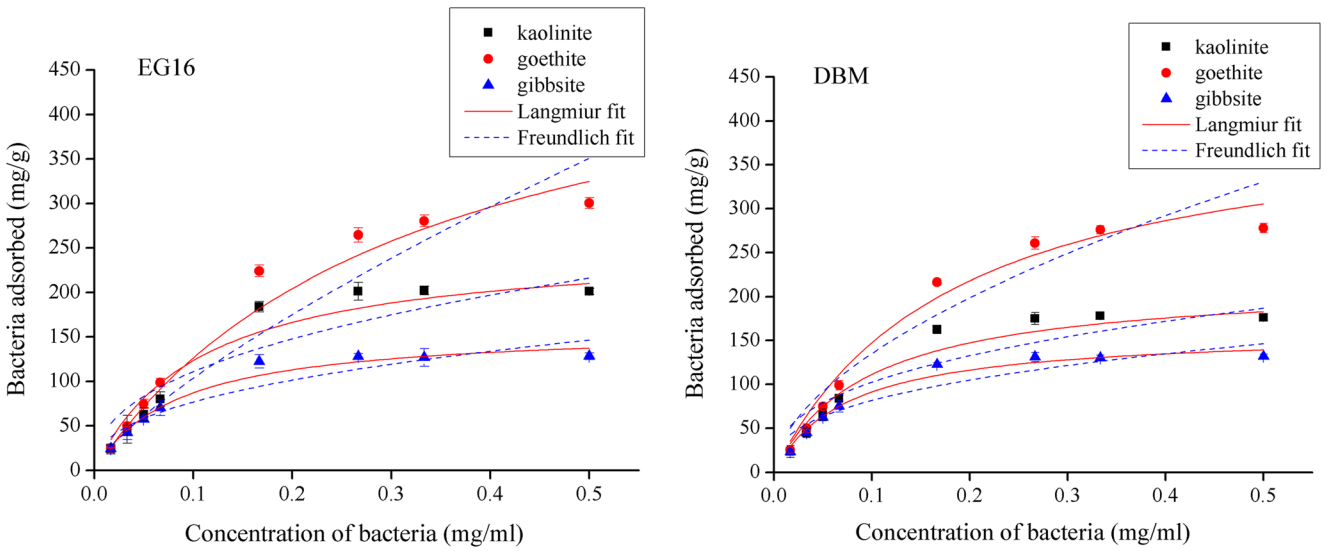

Fig. 3 Adsorption isotherms of bacteria (EG16 and DBM) and tested minerals (goethite, kaolinite, and gibbsite) combination

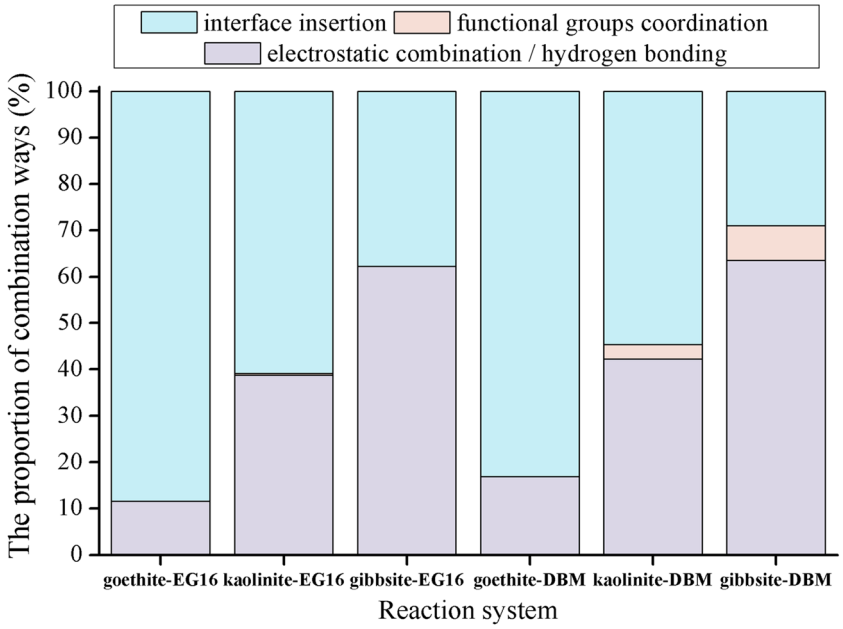

Fig. 4 Desorption of bacteria (EG16 and DBM) and minerals (goethite, kaolinite, and gibbsite) composites indicating different combined modes proportion

3.6 Scanning electron micrograph

From the SEM image a and b (Fig. 5), acicular goethite and flaky kaolinite agglomerated evidently and provided substantial voids for bacteria to get in. Differed from the status on the gibbsite surface, a large proportion of bacteria could be seen in SEM image d, e, g, and h, not only on the surface of goethite and kaolinite but also in the voids, which was consistent with the result of desorption. It can also be seen that the bacteria on the mineral surface tended to cluster together. Compared

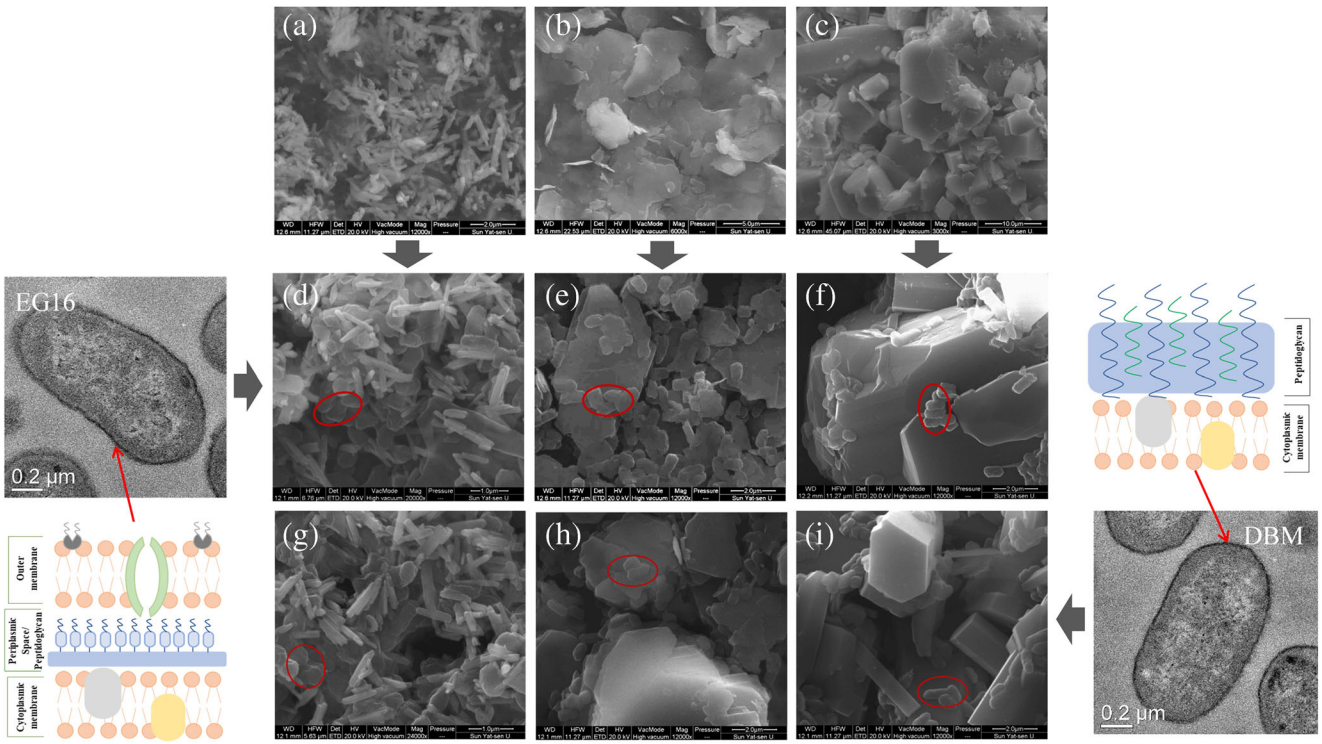

Fig. 5 SEM images of minerals (goethite, kaolinite, and gibbsite) and bacteria–mineral composites {**a**, goethite; **b**, kaolinite; **c**, gibbsite; **d**, EG16-goethite; **e**, EG16-kaolinite; **f**, EG16-gibbsite; **g**, DBM-goethite; **h**, DBM-kaolinite; **i**, DBM-gibbsite; examples of attached bacteria onto minerals marked in red circles; TEM and cell wall structure of EG16 and DBM are shown on the left and right sides respectively; the schematic diagram of bacterial cell wall structure is based on the description of Kulczycki (Kulczycki et al. 2002), Beveridge (Beveridge 1981), and Fang (Fang et al. 2009)}

composites images d–i with the mineral single component a–c, the agglomerated minerals loosen slightly after bacterial adhesion. Compared with the other two minerals, the smooth columnar structure of gibbsite may be more unfavorable for bacteria to attach.

3.7 Fourier transform infrared spectroscopy of bacteria–mineral composite

Compared with the spectra of goethite and bacteria, goethite–bacteria composites had involved the functional groups of both surfaces (Table 2, FigS4). The formation of composites mainly applied O–H bond from adsorbed water, bending -OH and free -OH on goethite surface, observed from shifting peaks at 1652 cm^{-1} (Rong et al. 2010), 1792 cm^{-1} (Ruan et al. 2001), and 3117 cm^{-1} (Wilson 1994), while partial DBM engaged into FeO_6 lattice, showing a shifting peak at 606 cm^{-1} (Wilson 1994). C–OH on peptidoglycan and N–H/C–N on amide were detected at the combination of both EG16 and DBM composites with goethite. Differed from DBM, EG16 also applied P=O double structure on outer membrane and C=O in the amide in the process of composite with goethite.

The formation of kaolinite–bacteria composites had significantly engaged the O–H bond in adsorbed water at 1636 cm^{-1} and 3449 cm^{-1}. Due to the layer structure of kaolinite, both bacteria chosen to attach to the Si–O bonds at 1114 cm^{-1} (Eren and Afsin 2008) and 698 cm^{-1} (Yuan et al. 2008) and Al–O bonds at 429 cm^{-1} (Saikia et al. 2003) from both sides of kaolinite, and partial EG16 also attached via the Al–OH bonds at 912 cm^{-1} (Yuan et al. 2008). Comparing two strains, EG16 mainly applied C=O and N–H or C–N in amide in the formation of kaolinite–bacteria composites, while DBM also engaged C–H bonds in protein alkyl at 2926 cm^{-1}.

For columnar gibbsite, bacteria mainly attached to Al–O bond at 450 cm^{-1} (Liu et al. 2012; Poorebrahimi and Norouzbeigi 2015), and EG16 also connected to Al–OH–Al bonds at 743 cm^{-1} (Poorebrahimi and Norouzbeigi 2015). Both bacteria attached to surface water instead of a structural -OH bond, while EG16 connected with variable H_2O with the peak near 2006 cm^{-1} and DBM with swinging H_2O with the peak near 665 cm^{-1}. P=O bonds on phospholipid, COO- in amino acids, C=O and N–H/C–N on amides, and C–H bonds in alkyl group (the peaks near 1236 cm^{-1}, 1396 cm^{-1}, 1544 cm^{-1}, 1656 cm^{-1}, 2926 cm^{-1} respectively) were engaged in the combination of bacteria–gibbsite composites, whereas EG16 showed more significant peak shifts of COO- and C–H bonds.

4 Discussion

Our results elucidated that electrostatic interaction played an essential role in bacterial adsorption on minerals. The first clue was that the adsorption of bacteria on minerals was markedly affected by pH. Increasing solution pH induces deprotonation on both bacteria and minerals surface, resulting in significantly decreasing zeta potentials of both materials. Therefore, the repulsive electrostatic force between kaolinite and bacteria increased, the attractive electrostatic force between goethite/gibbsite and bacteria reduced, and adsorption was hindered.

Data obtained at different ionic strengths also supported that electrostatic interaction was a significant contributor to bacterial adsorption on minerals. As presented in Fig. 1b and Fig. 2, zeta potential changes of bacteria and their adsorption trend onto tested minerals were consistent with the prediction of traditional DLVO theory (Hermansson 1999). For kaolinite and bacteria, which both are negatively charged, increasing ionic strength compressed the double electrode layer. This compression made the distance between kaolinite and bacteria closer, thus reducing the electrostatic repulsion and improving the adsorption performance. Positively charged minerals and bacteria, with lower ionic strength, have extensive diffusion layer and attractive electric fields, increasing the opportunities for adsorption. Once electrolyte accumulated, the compression of the diffusion layer of two surfaces reduces the electrostatic attraction (Cai et al. 2013). Also, a higher concentration of electrolyte ions could mask surface and limit the interaction between two surfaces. In other words, electrolyte ions could be a shield for electrostatic interaction blocking either attractive or repulsive force in higher ionic strength (Hong et al. 2018; Yee et al. 2000). Similar results have also been observed on bacterial adsorption by Fe-oxides (Hong et al. 2014), Al-oxides (Yee et al. 2000), and clay minerals (Zhao et al. 2012).

However, for negatively charged kaolinite and bacteria, which existing a strong electrostatic repulsion, substantial bacteria still adsorbed onto the kaolinite surface. Two speculations were made. On the one hand, kaolinite consists of double layers of oxides, $AlO(OH)_x$ and SiO_4. Point of zero charge (PZC) of Si–O as 3.0 means that for the tested pH range of 4–7, it served as a negatively charged surface while that of Al–O is 9.1 referred to a positively charged surface. Thus, the repulsion from the SiO_4 side may push the bacteria to the $AlO(OH)_x$ side, which explained the adsorption. This electrostatic force difference may also explain the spot cluster of bacteria on the kaolinite surface observed in SEM (Fig. 5 e, h). On the other hand, other non-electrostatic forces such as chemical interaction (chemical bonds/functional groups) and hydrogen bonding also play an essential role in the adsorption processes. The simulation of pseudo-second-order kinetic and Langmuir model (Fig. S3, Fig. 3 and Table 1) has sufficiently supported this. Pseudo-second-order kinetic model well fit the adsorption, indicating that chemical adsorption could be the rate-limiting step for the adsorption process of two bacteria on minerals (Dursun 2006). Likewise, well fit with the Langmuir model, the adsorption of bacteria on mineral is presented as

Table 2 Peak shifts in FTIR spectra before and after adsorption in ionic strength 0.01 M at pH 5

Single system	Functional group	Peaks (cm^{-1})	Peak shift (cm^{-1}) after adsorption					
			Goethite-EG16	Goethite-DBM	Kaolinite-EG16	Kaolinite-DBM	Gibbsite-EG16	Gibbsite-DBM
EG16	Stretching C–OH	1078	1063		–		–	
	Stretching P=O	1236	1231		–		1230	
	Stretching COO-	1396	–		–		1391	
	Bending CH_2	1453	–		–		–	
	AmideII/N–H/C–N	1544	1532		1543		1542	
	Stretching C=O	1656	1652		1653		1654	
	C–H bond	2926	–		–		2963	
	O–H or N–H	3302	–		–			
DBM	Stretching C–OH	1078		1060		–		–
	Stretching P=O	1236		–		–		1230
	Stretching COO-	1395		–		–		1393
	Bending CH_2	1455		–		–		–
	AmideII/N–H/C–N	1541		1540		–		1540
	Stretching C=O	1653		–		1654		–
	C–H bond	2926		–		2928		2928
	O–H or N–H	3304		–				
Goethite	FeO_6 lattice	607	–	606				
	Deformed Fe–OH	798	–	–				
		904	–	–				
	H_2O adsorbed V_2	1659	1652	1653				
	Bending -OH	1791	1792	1792				
	Free -OH	3117	3116	3115				
Kaolinite	Stretching Al–O	429			428	428		
	Deformed Si–O–Si	469			–	–		
	Stretching Al–O–Si	537			–	–		
	Stretching Si–O	698			697	697		
		794			–	–		
	Bending Al–OH	912			911	–		
	Stretching Si–O–Si	1006			–	–		
	Bending Si–O	1031			–	–		
	Quartz Si–O	1114			1115	1116		
	H_2O adsorbed V_2	1636			1653	1654		
	H_2O adsorbed V_1	3449			3422	3423		
	Structural -OH	3620			–	–		
	Stretching -OH	3696			–	–		
Gibbsite	Al–O	450					449	449
		516					–	515
		559					–	–
	Swinging H_2O	666					–	665
	Translational	743					742	–
	Al–OH–Al	799					–	–
	Deformed -OH	915					–	–
		968					–	–
		1021					–	–
	Variable H_2O	2007					2006	–
	Structural -OH	3526					–	–
		3621					–	–

Note: This table is arranged according to FTIR spectra. Characteristic peaks were listed as intrinsic functional groups, and shifted peaks of bacteria–mineral composites were listed as functional groups involved in the adsorption

single-layer chemical adsorption. The result of FTIR also proved it. FTIR spectra showed that the carboxyl, carbonyl, phosphate, and amino groups on the surface of bacteria and various hydroxyl groups on the surface of minerals were involved in the adsorption. The vibration of adsorbed water molecules on three mineral surfaces shifted after bacterial adsorption, which was generally regarded as the formation of hydrogen bond (Santhiya et al. 2001). These results confirmed that chemical interactions and hydrogen bonds are also crucial mechanisms governing the adhesion of bacteria onto kaolinite surface.

The results also showed significant variances in adsorption capacity among three tested minerals in the range of pH 4–7 and 1–100 mM KNO_3. This inconsistency of extent could

result from the structure and surface area difference of minerals and cell wall structure dissimilarities between Gram-positive and Gram-negative bacteria. SEM (Fig. 5) image and surface area data (Table S1) offered a shred of vivid evidence. It showed that acicular goethite with a large specific surface area was more favorable for bacteria to bind tightly. The smaller particle size and the lower zeta potential value of goethite favored aggregate formation, which provides substantial additional voids for bacterial insertion. Compared with goethite, kaolinite was a flaky structure with slightly smaller specific surface area, resulting in relatively minor adsorption. Due to its double-layer structure which serves opposite charges, bacteria tended to gather at the areas where present less repulsive force. For gibbsite, the smooth columnar structure with the smallest specific surface area makes the bacteria challenging to attach or insert.

The adsorption capacity of Gram-negative strain EG16 and Gram-positive strain DBM showed a bit different. The maximum capacities of EG16 on three tested minerals were 128.17%, 117.23%, and 100.29% of DBM, respectively. EG16 reflected higher calculated Q_{max}, except that on gibbsite. This difference can be attributed to the smaller size of EG16 (appr. 0.5 × 2 μm) compared to DBM (appr. 0.8 × 2 μm) that it could easily get into mineral voids and to the chemical component difference of cell wall (Fig. 5). The outer surface of Gram-positive bacteria is a thick layer of peptidoglycan, interluded with teichoic and lipoteichoic acid (Beveridge 1981; Fang et al. 2009; Kulczycki et al. 2002). Carboxyl (R-COO-, pK_a4.82), phosphate (R-PO-, pK_a6.9), and hydroxyl (R-O-, pK_a9.4) (Yee et al. 2000) could be the dominant functional groups on DBM surface. In our tested pH range, R-PO- and R-O- on bacterial surface tended to connect minerals through electrostatic force, while R-COO- connected that via complexation. Instead, Gram-negative bacteria are protected in a thin layer of peptidoglycan overlain by an outer lipid/protein bilayer with porins on it (Beveridge 1981; Fang et al. 2009; Kulczycki et al. 2002). The porins on its surface exposed the lipoprotein on periplasmic space and provided more hydrophilic amide for adsorption, which easy to form hydrogen bonds. Shortly, Gram-negative bacteria EG16 mainly attached to the mineral surface via inserting into the mineral voids and forming hydrogen bonds, and as for Gram-positive bacteria, chemical bonding also made contributions. The results of desorption have supported this.

It is worth noting that the carboxyl, carbonyl, and phosphate groups on the bacterial surface are also important active sites for heavy metal adsorption (Ngwenya et al. 2003). From our results of FTIR, it was evident that bacterial adhered to minerals occupied carboxyl, hydroxyl, and carbonyl on the bacterial surface and may mask some heavy metal adsorption sites, which inevitably affect the effectiveness of heavy metal immobilization of bacteria. However, from the desorption result (Fig. 4), the ratio of bacteria attached to minerals by functional groups was low, which presented the highest ratio of DBM-mineral as 7.46% and the lowest of EG16-mineral as 0.4%. Majority of bacteria attached to mineral through electrostatic force and inserting into voids; the masking sites covered by these connection forms may not be firmly occupied and possible to be used for metal absorption. Kulczycki et al. (2005) found an evidence that many active sites of bacteria masked by the attachment to ferrihydrite can be detected afterwards. Moreover, after combination, the absolute values of the zeta potential of bacteria–mineral composites were all below 20 mV, implying possible aggregation and favorable for metal immobilization. Shortly, it can be speculated that in bacteria–mineral combination, the occupied sites on the bacterial surface are limited, and those bacterial surface adhered to minerals via electrostatic force and inserting into voids can still have the potential to absorb heavy metals.

Besides minerals of interest in this study, soil organic matters could be another critical factor affecting the biosorption potential of metal-resistant bacteria (Zeng et al. 2011). On the one hand, organic matters could be glue connecting minerals and bacteria, forming larger aggregates and providing more active sites. On the other hand, it supplies organic chelates of different molecular sizes that can either immobilize heavy metal ions or increase metal bioavailability. Moreover, soil organic matter can be a source of nutrients for bacteria and plants, thus prolonging the sustainability of the system. As soil is a complicated black box, further experiments about the mineral–bacteria–plant ternary system should be carried out in future research for further understandings.

5 Conclusions

This study explored the adsorption behavior and mechanism of metal-resistant bacteria (Gram-negative EG16 and Gram-positive DBM) attaching to typical red soil minerals (goethite, kaolinite, and gibbsite) under different conditions and analyzed whether biosorption potential would be altered after the addition of functional bacteria to soil. The results showed that adsorption of bacteria onto gibbsite, kaolinite, and goethite were pH-dependent and for that onto goethite, ionic strength dependent as well, which can be well attributed to electrostatic force. All adsorption could be well described by pseudo-second-order kinetic model and Langmuir isothermal model, indicating chemical interaction (chemical bonds/functional groups) also play non-negligible roles in the adsorption. The result of FTIR and desorption experiment have adequately supported that. The adsorption capacity of Gram-negative strain EG16 was higher than that of Gram-positive strain DBM, and the attaching patterns of two bacteria to minerals were slightly different. Besides a small proportion of bacteria attached to minerals via functional groups, most

bacteria combined with minerals through electrostatic force. We could infer that the combination of bacteria and minerals has a limited impact on the potential of bacteria to adsorb heavy metals, and most of the bacteria adhered to minerals could still provide active sites for heavy metal biosorption.

Acknowledgments The authors are grateful to the reviewers who help us improve the paper by many pertinent comments and suggestions.

Funding information This work was supported by the National Key Research and Development Program (2018YFD0800700), the Youth Program of National Natural Science Foundation of China (41807031), Natural Science Foundation of Guangdong Province (2018A030310127), and China Postdoctoral Science Foundation Funded Project (2018M643309).

Compliance with ethical standards

Conflict of interest The authors declare that they have no conflict of interest.

References

Ams DA, Fein JB, Dong H, Maurice PA (2004) Experimental measurements of the adsorption of *Bacillus subtilis* and *Pseudomonas mendocina* onto Fe-oxyhydroxide-coated and uncoated quartz grains. Geomicrobiol J 21:511–519. https://doi.org/10.1080/01490450490888172

Bai J, Yang X, Du R, Chen Y, Wang S, Qiu R (2014) Biosorption mechanisms involved in immobilization of soil Pb by *Bacillus subtilis* DBM in a multi-metal-contaminated soil. J Environ Sci (China) 26:2056–2064. https://doi.org/10.1016/j.jes.2014.07.015

Belimov AA, Hontzeas N, Safronova VI, Demchinskaya SV, Piluzza G, Bullitta S, Glick BR (2005) Cadmium-tolerant plant growth-promoting bacteria associated with the roots of Indian mustard (*Brassica juncea* L. Czern.). Soil Biol Biochem 37:241–250. https://doi.org/10.1016/j.soilbio.2004.07.033

Beveridge TJ (1981) Ultrastructure, chemistry, and function of the bacterial wall. Int Rev Cytol 72:229–317. https://doi.org/10.1016/s0074-7696(08)61198-5

Cai P, Huang Q, Walker SL (2013) Deposition and survival of *Escherichia coli* O157:H7 on clay minerals in a parallel plate flow system. Environ Sci Technol 47:1896–1903. https://doi.org/10.1021/es304686a

Cao Y, Wei X, Cai P, Huang Q, Rong X, Liang W (2011) Preferential adsorption of extracellular polymeric substances from bacteria on clay minerals and iron oxide. Colloids Surf B Biointerfaces 83:122–127. https://doi.org/10.1016/j.colsurfb.2010.11.018

Chatterjee S, Sau GB, Mukherjee SK (2009) Plant growth promotion by a hexavalent chromium reducing bacterial strain, *Cellulosimicrobium cellulans* KUCr3. World J Microbiol Biotechnol 25:1829–1836. https://doi.org/10.1007/s11274-009-0084-5

Chen Y et al (2016a) Survival strategies of the plant-associated bacterium *Enterobacter* sp. strain EG16 under cadmium stress. Appl Environ Microbiol 82:1734–1744. https://doi.org/10.1128/AEM.03689-15

Chen Y, Yang W, Chao Y, Wang S, Tang Y-T, Qiu R-L (2016b) Metal-tolerant *Enterobacter* sp. strain EG16 enhanced phytoremediation using *Hibiscus cannabinus* via siderophore-mediated plant growth promotion under metal contamination. Plant Soil 413:203–216. https://doi.org/10.1007/s11104-016-3091-y

Cheng PF, Wang Y, Cheng K, Li FB, Qin HL, Liu TX (2017) The acid base buffer capacity of red soil variable charge minerals and its surface complexation model. Acta Chim Sinica 75:637–644. https://doi.org/10.6023/A17020056

Das SK, Guha AK (2007) Biosorption of chromium by *Termitomyces clypeatus*. Colloids Surf B Biointerfaces 60:46–54 https://doi.org/10.1016/j.colsurfb.2007.05.021

Doshi H, Ray A, Kothari IL (2007) Biosorption of cadmium by live and dead *Spirulina*: IR spectroscopic, kinetics, and SEM studies. Curr Microbiol 54:213–218. https://doi.org/10.1007/s00284-006-0340-y

Dursun AY (2006) A comparative study on determination of the equilibrium, kinetic and thermodynamic parameters of biosorption of copper(II) and lead(II) ions onto pretreated *Aspergillus niger*. Biochem Eng J 28:187–195. https://doi.org/10.1016/j.bej.2005.11.003

Eren E, Afsin B (2008) An investigation of cu(II) adsorption by raw and acid-activated bentonite: a combined potentiometric, thermodynamic, XRD, IR, DTA study. J Hazard Mater 151:682–691. https://doi.org/10.1016/j.jhazmat.2007.06.040

Fang L, Cai P, Chen W, Liang W, Hong Z, Huang Q (2009) Impact of cell wall structure on the behavior of bacterial cells in the binding of copper and cadmium. Colloids Surf Physicochem Eng Aspects 347:50–55. https://doi.org/10.1016/j.colsurfa.2008.11.041

Fang L et al (2011) Binding characteristics of copper and cadmium by cyanobacterium *Spirulina platensis*. J Hazard Mater 190:810–815. https://doi.org/10.1016/j.jhazmat.2011.03.122

Hermansson M (1999) The DLVO theory in microbial adhesion. Colloids Surf B Biointerfaces 14:105–119. https://doi.org/10.1016/s0927-7765(99)00029-6

Hong ZN, Zhao G, Chen WL, Rong XM, Cai P, Dai K, Huang QY (2014) Effects of solution chemistry on bacterial adhesion with phyllosilicates and goethite explained by the extended DLVO theory. Geomicrobiol J 31:419–430. https://doi.org/10.1080/01490451.2013.824523

Hong ZN, Jiang J, Li JY, Xu RK (2018) Preferential adhesion of surface groups of *Bacillus subtilis* on gibbsite at different ionic strengths and pHs revealed by ATR-FTIR spectroscopy. Colloids Surf B Biointerfaces 165:83–91. https://doi.org/10.1016/j.colsurfb.2018.02.020

Jiang D, Huang Q, Cai P, Rong X, Chen W (2007) Adsorption of *Pseudomonas putida* on clay minerals and iron oxide. Colloids Surf B Biointerfaces 54:217–221. https://doi.org/10.1016/j.colsurfb.2006.10.030

Joshi PM, Juwarkar AA (2009) In vivo studies to elucidate the role of extracellular polymeric substances from *Azotobacter* in immobilization of heavy metals. Environ Sci Technol 43:5884–5889. https://doi.org/10.1021/es900063b

Juwarkar AA, Nair A, Dubey KV, Singh SK, Devotta S (2007) Biosurfactant technology for remediation of cadmium and lead contaminated soils. Chemosphere 68:1996–2002. https://doi.org/10.1016/j.chemosphere.2007.02.027

Kulczycki E, Ferris FG, Fortin D (2002) Impact of cell wall structure on the behavior of bacterial cells as sorbents of cadmium and lead. Geomicrobiol J 19:553–565. https://doi.org/10.1080/01490450290098586

Kulczycki E, Fowle DA, Fortin D, Ferris FG (2005) Sorption of cadmium and lead by bacteria–ferrihydrite composites. Geomicrobiol J 22:299–310. https://doi.org/10.1080/01490450500184694

Liu CC et al (2010) Mineral magnetism to probe into the nature of palaeomagnetic signals of subtropical red soil sequences in southern. China GeoJI 181:1395–1410. https://doi.org/10.1111/j.1365-246X.2010.04592.x

Liu LJ, Xu FY, Yu ZL, Dong P (2012) Facile fabrication of non-sticking superhydrophobic boehmite film on Al foil. Appl Surf Sci 258:8928–8933. https://doi.org/10.1016/j.apsusc.2012.05.119

Loukidou MX, Zouboulis AI, Karapantsios TD, Matis KA (2004) Equilibrium and kinetic modeling of chromium(VI) biosorption by *Aeromonas caviae*. Colloids Surf Physicochem Eng Aspects 242: 93–104. https://doi.org/10.1016/j.colsurfa.2004.03.030

Lu Y et al (2015) Impacts of soil and water pollution on food safety and health risks in China. Environ Int 77:5–15. https://doi.org/10.1016/j.envint.2014.12.010

Luo SL et al (2011) Analysis and characterization of cultivable heavy metal-resistant bacterial endophytes isolated from Cd-hyperaccumulator *Solanum nigrum* L. and their potential use for phytoremediation. Chemosphere 85:1130–1138. https://doi.org/10.1016/j.chemosphere.2011.07.053

Ma Y, Rajkumar M, Luo YM, Freitas H (2011) Inoculation of endophytic bacteria on host and non-host plants–effects on plant growth and Ni uptake. J Hazard Mater 195:230–237. https://doi.org/10.1016/j.jhazmat.2011.08.034

Moon EM, Peacock CL (2013) Modelling Cu(II) adsorption to ferrihydrite and ferrihydrite-bacteria composites: deviation from additive adsorption in the composite sorption system. Geochim Cosmochim Acta 104:148–164. https://doi.org/10.1016/j.gca.2012.11.030

Nath J, Ray L (2015) Biosorption of Malachite green from aqueous solution by dry cells of *Bacillus cereus* M-16(1) (MTCC 5521). J Environ Chem Eng 3:386–394. https://doi.org/10.1016/j.jece.2014.12.022

Ngwenya BT, Sutherland IW, Kennedy L (2003) Comparison of the acid-base behaviour and metal adsorption characteristics of a gram-negative bacterium with other strains. Appl Geochem 18:527–538. https://doi.org/10.1016/S0883-2927(02)00118-X

Poorebrahimi S, Norouzbeigi R (2015) A facile solution-immersion process for the fabrication of superhydrophobic gibbsite films with a binary micro-nano structure: effective factors optimization via Taguchi method. Appl Surf Sci 356:157–166. https://doi.org/10.1016/j.apsusc.2015.07.172

Rajkumar M, Sandhya S, Prasad MN, Freitas H (2012) Perspectives of plant-associated microbes in heavy metal phytoremediation. Biotechnol Adv 30:1562–1574. https://doi.org/10.1016/j.biotechadv.2012.04.011

Rong X, Huang Q, He X, Chen H, Cai P, Liang W (2008) Interaction of *Pseudomonas putida* with kaolinite and montmorillonite: a combination study by equilibrium adsorption, ITC, SEM and FTIR. Colloids Surf B Biointerfaces 64:49–55. https://doi.org/10.1016/j.colsurfb.2008.01.008

Rong X, Chen W, Huang Q, Cai P, Liang W (2010) *Pseudomonas putida* adhesion to goethite: studied by equilibrium adsorption, SEM, FTIR and ITC. Colloids Surf B Biointerfaces 80:79–85. https://doi.org/10.1016/j.colsurfb.2010.05.037

Ruan HD, Frost RL, Kloprogge JT (2001) The behavior of hydroxyl units of synthetic goethite and its dehydroxylated product hematite. Spectrochim Acta A Mol Biomol Spectrosc 57:2575–2586. https://doi.org/10.1016/s1386-1425(01)00445-0

Saikia NJ, Bharali DJ, Sengupta P, Bordoloi D, Goswamee RL, Saikia PC, Borthakur PC (2003) Characterization, beneficiation and utilization of a kaolinite clay from Assam, India. Appl Clay Sci 24:93–103. https://doi.org/10.1016/S0169-1317(03)00151-0

Santhiya D, Subramanian S, Natarajan KA (2001) Surface chemical studies on sphalerite and galena using *Bacillus polymyxa*. J Colloid Interface Sci 235:298–309. https://doi.org/10.1006/jcis.2000.7256

Sinha S, Mukherjee SK (2008) Cadmium-induced siderophore production by a high Cd-resistant bacterial strain relieved Cd toxicity in plants through root colonization. Curr Microbiol 56:55–60. https://doi.org/10.1007/s00284-007-9038-z

Turgay OC, Bilen S (2012) The role of plant growth-promoting rhizosphere bacteria in toxic metal extraction by *Brassica* spp. https://doi.org/10.1007/978-94-007-3913-0_8

Ueshima M, Ginn BR, Haack EA, Szymailowski JES, Fein FB (2008) Cd adsorption onto *Pseudomonas putida* in the presence and absence of extracellular polymeric substances. Geochim Cosmochim Acta 72: 5885–5895. https://doi.org/10.1016/j.gca.2008.09.014

Vivas A, Biro B, Ruiz-Lozano JM, Barea JM, Azcon R (2006) Two bacterial strains isolated from a Zn-polluted soil enhance plant growth and mycorrhizal efficiency under Zn-toxicity. Chemosphere 62:1523–1533. https://doi.org/10.1016/j.chemosphere.2005.06.053

Wang Q, Xiong D, Zhao P, Yu X, Tu B, Wang G (2011) Effect of applying an arsenic-resistant and plant growth-promoting rhizobacterium to enhance soil arsenic phytoremediation by *Populus deltoides* LH05-17. J Appl Microbiol 111:1065–1074. https://doi.org/10.1111/j.1365-2672.2011.05142.x

Wang N, Du HH, Huang QY, Cai P, Rong XM, Feng XH, Chen WL (2016) Surface complexation modeling of Cd(II) sorption to montmorillonite, bacteria, and their composite. Biogeosciences 13:5557–5566. https://doi.org/10.5194/bg-13-5557-2016

Wang L, Ji B, Hu Y, Liu R, Sun W (2017) A review on in situ phytoremediation of mine tailings. Chemosphere 184:594–600. https://doi.org/10.1016/j.chemosphere.2017.06.025

Wilson MJ (1994) Clay mineralogy: spectroscopic and chemical determinative methods. 10.1007/978-94-011-0727-3

Yee N, Fein JB, Daughney CJ (2000) Experimental study of the pH, ionic strength, and reversibility behavior of bacteria-mineral adsorption. Geochim Cosmochim Acta 64:609–617. https://doi.org/10.1016/S0016-7037(99)00342-7

Yuan P, Annabi-Bergaya F, Tao Q, Fan M, Liu Z, Zhu J, He H, Chen T (2008) A combined study by XRD, FTIR, TG and HRTEM on the structure of delaminated Fe-intercalated/pillared clay. J Colloid Interface Sci 324:142–149. https://doi.org/10.1016/j.jcis.2008.04.076

Zeng F, Ali S, Zhang H, Ouyang Y, Qiu B, Wu F, Zhang G (2011) The influence of pH and organic matter content in paddy soil on heavy metal availability and their uptake by rice plants. Environ Pollut 159:84–91. https://doi.org/10.1016/j.envpol.2010.09.019

Zhang TX, Yang WH, Zhu XY, Wang HZ, Brookes PC, Xu J (2014) The pH dependence of *Escherichia coli* O157:H7 adsorption on kaolinite and goethite surfaces. J Soils Sediments 15:106–116. https://doi.org/10.1007/s11368-014-0948-7

Zhao WQ, Liu X, Huang QY, Walker SL, Cai P (2012) Interactions of pathogens *Escherichia coli* and *Streptococcus suis* with clay minerals. Appl Clay Sci 69:37–42. https://doi.org/10.1016/j.clay.2012.07.003